ACS OMEGA

http://pubs.acs.org/journal/acsodf

Article

# Enhanced Tetracycline Removal from Highly Concentrated Aqueous Media by Lipid-Free *Chlorella* sp. Biomass

Dayra Suárez-Martínez, Edgardo Angulo-Mercado, Ivan Mercado-Martínez, Victor Vacca-Jimeno, Claudia Tapia-Larios, and Néstor Cubillán*

Cite This: *ACS Omega* 2022, 7, 14128−14137

Read Online

ACCESS | Metrics & More | Article Recommendations | Supporting Information

**ABSTRACT:** Microalgae are used as a lipid source for different applications, such as cosmetics and biofuel. The nonliving biomass and the byproduct from the lipid extraction procedure can efficiently remove antibiotics. This work has explored the potential use of *Chlorella* sp. biomasses for tetracycline (**Tc**) removal from highly concentrated aqueous media. Non-living biomass (NLB) is the biomass before the lipid extraction procedure, while lipid-extracted biomass (LEB) is the byproduct mentioned before. LEB removed 76.9% of **Tc** at 40 mg/L initial concentration and 40 mg of biomass, representing an adsorption capacity of 19.2 mg/g. Subsequently, NLB removed 68.0% of **Tc** at 50 mg/L and 60 mg of biomass, equivalent to 14.2 mg/g of adsorptive capacity. These results revealed an enhanced removal capacity by LEB compared with NLB and other microalgae-based materials. On the other hand, the adsorption kinetics followed the pseudo-second-order and Elovich models, suggesting chemisorption with interactions between adsorbates. The adsorption isotherms indicate a multilayer mechanism on a heterogeneous surface. Additionally, the interactions between the surface and the first layer of tetracycline are weak, and the formation of the subsequent layers is favored. The *Chlorella* sp. biomass after the lipid extraction process is a promising material for removing tetracycline; moreover, the use of this residue contributes to the zero-waste strategy.

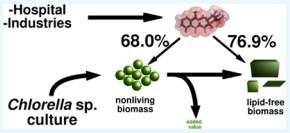


## 1. INTRODUCTION

Tetracyclines are the second most widely used antibiotics class produced and sold worldwide. They are broad-spectrum antibiotics used to treat infectious diseases generated by Gram-positive and Gram-negative microorganisms in animals and humans.[1] In many countries of the European Union, these substances are most often used (37%) in veterinary medicine.[2]

In several low- and medium-income—and some high-income—countries, the legislation about antibiotic use is weak or inexistent, and self-medication contributes to the spill-out problem. Tetracycline (**Tc**) is still used in animal production for growth promotion in these countries.[3] Several studies show **Tc** is not completely absorbed, and the rest is eliminated through urine and feces, for example, the bioavailability of **Tc** in broiler chickens is 56.45% ± 9.71.[4]

Based on this information, it is not surprising that **Tc** is one of the most abundant drugs in wastewater.[5] In Iran, concentrations between 5.4 and 8.1 ng/L were found in wells and dams adjacent to the farming houses of Tehran. The authors attributed these levels in the water resources to the municipal wastewater treatment plant effluents where concentrations of tetracycline ranged from 280 to 540 ng/L.[6] Additionally, Wang et al. found 11.68 ng/L of **Tc** in the drinking water sources of the lower Yangtze River. The main sources of **Tc** were the tributary rivers (74.5%) and sewage discharges (25.5%).[7]

The persistence of antibiotics in water sources promotes the appearance of antibiotic-resistant microorganisms; for example, in 335 samples of *Enterococcus faecalis* from retail chicken meats, 149 were tetracycline resistant.[8] This situation represents a public health problem. A strategy for decreasing **Tc** presence can be carried out by removing the antibiotic from effluents with high concentration, that is, production, industrial, hospital, and agriculture wastewater. In these effluents, the **Tc** concentration ranged between $\mu$g/L and mg/L.[9−11] The wastewater treatment plants for these influents do not have the procedures to remove tetracycline-family drugs.[12]

Despite the ongoing efforts, research on **Tc** removal technology for this concentration range is still necessary. Techniques such as advanced oxidation processes, coagulation, ion exchange, and adsorption showed high efficiencies removing **Tc**. Fenton oxidation reached ca. 90% removal efficiency.[13] Zhang et al. found 95.6% of **Tc** decreasing using a 3D biofilm-electrode reactor.[14] In the same way, the adsorption-based processes with advanced materials have given good results. The Fe-doped graphene oxide[15] and multiwalled carbon nanotubes[16] were capable of removing 98 and 99.8%, respectively. Despite the effectiveness of these methods, in low- and medium-income countries, the costs of

**Received:** February 3, 2022
**Accepted:** April 5, 2022
**Published:** April 14, 2022

oxidation technologies and advanced adsorption materials can be unreachable.

A simple, low-cost, and efficient method is microalgae-based technology. These living microorganisms are essential in oxidation ponds for wastewater treatments. The nonliving biomass is a byproduct of the involved processes from the microalgae life cycle. The biomass is a source of several compounds that an added value can be obtained, for example, lipids (5.5−73.9%), proteins (10.2−47.4%), and polysaccharides (9.7−30.3%).[17] Particularly, *Chlorella* sp. is considered a species with high lipid concentration, containing between 30 and 70% of lipids.[18]

The application of the extracted lipids ranged from cosmetic to food industries.[19] The economic profit can reach 100 €/kg for each high value-added compound.[20] The biomass production costs are about 2.71 US$/kg[21] and can be reduced by 55%, improving the feeding[22] and harvesting processes. The byproduct obtained after the lipid extraction procedure is rich in polysaccharides and proteins. This lipid-extracted biomass (LEB) had no known application. The waste disposal costs around €0.03/kg when it is not contaminated and up to €0.20/kg if it is considered hazardous waste.

In both nonliving biomasses, before and after lipid extraction, the porous and heterogeneous surface and interstices and the diversity in functional groups suggest a potential capacity to remove the contaminants. Their sustainability, low toxicity, and costs represent advantages over advanced adsorption technologies from an operational viewpoint.[23] The applicability of the nonliving microalgae biomass and their physical and chemical modifications in pharmaceuticals removal is widely documented.[24,25]

Despite the facts mentioned above, the nonliving biomasses as antibiotic removal materials have little presence in the literature. Angulo et al. found 82.7% of cephalexin removal with nonliving *Chlorella* sp. biomass, and 71.2% was observed with the biomass modified by lipid extraction.[26] Moreover, Daneshvar et al. found 62.97 and 55.11% at 80 mg/L of **Tc** removal efficiencies with lipid-free biomass of *Scenedesmus quadricauda* and *Tetraselmis suecica*, respectively.[27] In recent work, Saldaña et al. reported 90.8 and 80.8% of minocycline removal with the nonliving *Chlorella* sp. and the lipid-free biomasses, respectively.[28] Therefore, removing the antibiotics by nonliving microalgae, lipid-free biomass remains in initial stages.

In our group, there is an interest in

1) Exploring the potential use of nonliving *Chlorella* sp. biomasses—before and after lipid extraction—for antibiotic removal in highly concentrated aqueous media,
2) Suggesting bioadsorption mechanisms through the kinetics and isotherm analysis, and
3) Establishing relations between antibiotic structure and removal capacity.

In this regard, a comparison of **Tc** removal by nonliving *Chlorella* sp. biomasses before and after lipid extraction is presented.

## 2. MATERIALS AND METHODS

**2.1. Nonliving and Lipid-Extracted *Chlorella* sp. Biomass Preparation.** Microalgae Biotechnology Laboratory at Universidad del Atlántico (Barranquilla, Colombia) provided the *Chlorella* sp. strains. The living microorganisms were cultured in triplicates in a sterilized glass container. The culture media was a solution of the commercial NPK fertilizer (Nutrifoliar, Colinagro, Colombia) diluted to give 1.0 mmol/L of nitrogen. The *Chlorella* sp. was added to obtain an absorbance of 0.100 units (UV-1800, Shimadzu, Japan) at 647 nm. The temperature was kept at 27 ± 2 °C for 20 days with constant shaking and aeration (2.5 L/min, Power Life, USA). The light intensity was 86.2 ± 5 $\mu$mol/m$^2$ s (Ingeolux led lamps, Colombia) and photoperiods (12 h light/12 h darkness).

After growth, the aeration and lighting system were powered off. Three days later, the cultures were centrifuged (Hettich, Rotofix 32 A, Germany) at 3000 rpm by 7 min. The biomass was washed several times with distilled water and dried in a heating oven at 70 °C for 12 h. Finally, it was pulverized and stored.[29] The resulting biomass was called "nonliving *Chlorella* sp. biomass" and abbreviated starting now NLB.

The lipids were extracted from NLB by a modification of Bligh and Dyer,[30] and Guo et al.[31] protocols: 10 mL of a 2:1 chloroform:methanol (Merck, 99.8%, USA) mixture was added to 50 mg of NLB, sonicated (VWR B1500A-MT, Ultrawave, UK) for 1 h, and homogenized for 30 s after the addition of NaCl solution (Panreac, 0.9% w/v, Spain). Finally, the mixture was centrifuged (3000 rpm, 8 min), and the organic phase was filtered (1882-047, Whatman, USA). Furthermore, a Soxhlet extraction with hexane (Merck, 97%, USA) was conducted for 5 h (siphon rate of 8−10 cycles/h).[32] The residual biomass was isolated and washed with 2:1 chloroform:methanol (Merck, 99.8%, USA) mixture. This biomass is called "lipid-extracted *Chlorella* sp. biomass" and henceforth abbreviated LEB.

The adsorbent characterization was carried out by Fourier-transform infrared spectroscopy with an attenuated total reflection device (FTIR-ATR, Bruker, Tensor II, Germany) and scanning electron microscopy (SEM, Quanta FEG 650, FEI, USA). The samples stubs were fixed with carbon adhesive tape and sputtered with gold.

The FTIR-ATR technique showed proteins (1650, 1550, and 1400−1200 cm$^{-1}$) and carbohydrates (1050 cm$^{-1}$) in both biomasses. The phospholipids, fatty acids, and lipids appeared around 1250 and 1730−1750 cm$^{-1}$. With the lipid extraction procedure, the bands assigned to carbohydrate and phospholipids decreased intensity, and the lipid and fatty acids bands disappeared.

On the other hand, SEM revealed different morphology for NLB (globular) and LEB (flakes and blocks). The size distribution was also different, between 20 and 50 $\mu$m in NLB and 2 and 400 $\mu$m for LEB.[28]

**2.2. Maximum-Removal Conditions and Calibration Curves.** The maximum-removal conditions were determined by evaluating the pH,[2−6,8−12] concentration of **Tc** (Genfar, HPLC purity >98%, Colombia) [$C_0$ (mg/L): 40, 50, 60] and sorbent mass, $m$ (mg): 40, 50, 60). A D-optimal experimental design gave the experiment's grid by maximizing the $D$-value through the Federov optimization. The *AlgDesign* library in the R program[33,34] assisted these calculations. We have considered a linear model of the three variables (as factors) without interaction, and Table 1 contains the resulting experiments.

The rows in Table 1 show the variable values for each experiment. The aqueous **Tc** solution (25 mL) and the biomass were mixed, shaken (Digital Orbital Shaker, 200 rpm, 6 h), and centrifuged (Hettich, Rotofix 32) at 3500 rpm. The absorbance of the supernatant at 1 min ($A_i$) and 6 h ($A_f$)


https://doi.org/10.1021/acsomega.2c00696
ACS Omega 2022, 7, 14128−14137

Table 1. Grid of Experiments To Evaluate the Maximum-Removal Conditions[a]

| experiment | pH | $m$ (mg) | $C_0$ (mg/L) |
|---|---|---|---|
| 1 | 2 | 40 | 60 |
| 2 | 2 | 50 | 50 |
| 3 | 2 | 60 | 40 |
| 4 | 3 | 40 | 40 |
| 5 | 3 | 50 | 50 |
| 6 | 3 | 60 | 60 |
| 7 | 4 | 40 | 40 |
| 8 | 4 | 50 | 50 |
| 9 | 4 | 60 | 60 |
| 10 | 5 | 40 | 40 |
| 11 | 5 | 50 | 50 |
| 12 | 5 | 60 | 60 |
| 13 | 6 | 40 | 40 |
| 14 | 6 | 50 | 50 |
| 15 | 6 | 60 | 60 |
| 16 | 8 | 40 | 40 |
| 17 | 8 | 50 | 50 |
| 18 | 8 | 60 | 60 |
| 19 | 9 | 40 | 40 |
| 20 | 9 | 50 | 50 |
| 21 | 9 | 60 | 60 |
| 22 | 10 | 40 | 40 |
| 23 | 10 | 50 | 50 |
| 24 | 10 | 60 | 60 |
| 25 | 11 | 40 | 50 |
| 26 | 11 | 50 | 40 |
| 27 | 11 | 60 | 60 |
| 28 | 12 | 40 | 40 |
| 29 | 12 | 50 | 50 |
| 30 | 12 | 60 | 60 |

[a] $m$, biomass mass; $C_0$, **Tc** initial concentration.

defined the apparent removal ($\%R_{ap}$), and it was calculated with eq 1:

$$\%R_{ap} = \frac{A_i - A_f}{A_i} \times 100\% \quad (1)$$

where $A_i$ and $A_f$ are the initial and final absorbance of the maximum-absorbance band, respectively. The results of $\%R_{ap}$ were fitted by multiple linear regression with pH, $C_0$, and $m$ as variables in a quadratic equation with interactions:

$$\%R_{ap} = \%R_{ap}^0 + m + C_0 + \mathrm{pH} + m^2 + C_0^2 + \mathrm{pH}^2 + m{\cdot}C_0 + m{\cdot}\mathrm{pH} + C_0{\cdot}\mathrm{pH} + m{\cdot}C_0^2 + m^2{\cdot}C_0 + m{\cdot}\mathrm{pH}^2 + m^2{\cdot}\mathrm{pH} + \mathrm{pH}{\cdot}C_0^2 + \mathrm{pH}^2{\cdot}C_0 \quad (2)$$

The significant variables were selected by an "all subsets" procedure and the nonsignificant variable was depreciated. The influence of pH, $C_0$, and $m$ and their interactions were discussed in terms of the variable significance in the model.

Furthermore, the calibration curves and experiments were conducted with variable values where $\%R_{ap}$ was maximum. The **Tc** concentrations for the calibration curves were 20, 25, 30, 35, 40, 45, 50, 55, and 60 mg/L. An ANCOVA analysis evaluated the biomass effect on the calibration curve. The biomass content was a factor with three levels: without (treatment 0) and with biomass (nonliving biomass: treatment 1; nonliving lipid-extracted biomass: treatment 2).

### 2.3. Removal Time-Profiles and Adsorption Kinetics.

A 25 mL of **Tc** solution was prepared with the initial concentration, biomass mass, and pH value, where $\%R_{ap}$ was a maximum. The absorbance at several times (1, 15, 30, 60, 120, 180, 240, 300, and 360 min) let it calculate the concentrations ($C_t$, mg/L). Furthermore, the adsorption capacity ($q_t$) and the removal efficiency ($\%R$) are calculated:

$$q_t = (C_0 - C_t)\frac{V}{m_b} \quad (3)$$

$$\%R = \left(\frac{C_0 - C_t}{C_0}\right) \times 100\% \quad (4)$$

where $C_0$ is the concentration at time zero. $V$ is the solution volume (0.025 L) of the tetracycline solution and $m_b$ is the biomass mass (mg).

The fitting of $q_t$ data described the adsorption kinetics. The models of pseudo-first-order (eq 5), pseudo-second order (eq 6), Elovich (eq 7), and intraparticle diffusion (eq 8) were considered.

$$q_t = q_e(1 - e^{-k_1 t}) \quad (5)$$

$$q_t = \frac{q_e^2 k_2 t}{1 + q_e k_2 t} \quad (6)$$

$$q_t = \frac{1}{\beta}\ln(1 + \alpha\beta t) \quad (7)$$

$$q_t = k_p t^{1/2} + C \quad (8)$$

Here, $q_e$ (mg·g$^{-1}$) is the equilibrium adsorption capacity. $k_1$ (min$^{-1}$) and $k_2$ (g·mg$^{-1}$·min) are pseudo-first and pseudo-second-order rate constants. In the Elovich equation, $\alpha$ (mg·g$^{-1}$·min$^{-1}$) is the initial rate constant, and $\beta$ (mg·g$^{-1}$) is the desorption constant. For the intraparticle diffusion model, $K_p$ is the rate constant, and $C$ is a constant proportional to the extent of the boundary layer thickness.[35]

$R$[34] was the software to calculate $q_t$ data's linear and nonlinear fitting. The determination coefficient ($R^2$) was the goodness-of-fit criteria to evaluate the adequacy of data to a model.

### 2.4. Adsorption Equilibrium.

The experiments were conducted at pH value and biomass quantity, where the maximum removal occurred (Section 2.2). The contact time was determined by kinetic studies (Section 2.3). 25 mL of **Tc** solution with the biomass was shaken (150 rpm) in triplicate at 25 °C. The calibration curves give the concentrations using the absorbance recorded before and after stirring. These results were fitted to the Freundlich (eq 9), Brunauer–Emmet–Teller (BET, eq 10) and Frenkel–Halsey–Hill (FHH, eq 11) isotherms:

$$q_e = K_f C_e^{1/n} \quad (9)$$

$$q_e = \frac{q_{max} C_{BET} C_e / C_s}{(1 - C_e/C_s)(1 - C_e/C_s + C_{BET} C_e/C_s)} \quad (10)$$

$$q_e = \left(\frac{-1}{A_{fhh}}\ln\left(\frac{C_e}{C_s}\right)\right)^{-1/B_{fhh}} \quad (11)$$



https://doi.org/10.1021/acsomega.2c00696
ACS Omega 2022, 7, 14128−14137

where $K_f$ is the Freundlich equilibrium constant, $C_e$ is the equilibrium concentration ($mg \cdot L^{-1}$), and $1/n$ is related to the adsorbate−adsorbent affinity. In eq 10, $q_{max}$ is the maximum adsorption capacity, $C_{BET}$ is the BET constant, and $C_s$ is the saturation concentration. In eq 11, $A_{fhh}$ and $B_{fhh}$ are constants indicating the affinity of adsorbate by the adsorbent and the interaction between the surface and subsequent adsorbate layers, respectively.

Three algorithms conducted the data fitting: ordinary least squares for the linearized equation (Freundlich model), the Gauss-Newton for the nonlinear equation (Freundlich model), and genetic algorithms (population = 1000, generations = 1000, crossover rate = 50%, mutation rate = 10%) followed by optimization with the Broyden−Fletcher−Goldfarb−Shanno algorithm (BET and FHH models).[36]

**2.5. Density Functional Theory Calculations.** Jin et al.[37] described the prototropic species of tetracycline. In this work, we have calculated the molecular electrostatic potential of these species to explain the possible intermolecular interactions drawing the adsorption process. The electronic structure calculations were realized in the density functional theory (DFT) at M06-2X/6-311 + g(d,p) level of theory. The geometry of the structures was optimized. Additionally, the absence of negative frequencies from the vibrational analysis confirmed the finding of a local minimum in the potential energy surface. All calculations were performed with Gaussian 09 Rev. A02.[38]

## 3. RESULTS AND DISCUSSION

**3.1. Maximum-Removal Conditions and Calibration Curves.** Figure 1 shows the response surface for the apparent **Tc** removal with NLB and LEB. The apparent **Tc** removal increases with the increasing pH in both biomasses. Additionally, the biomass dosage and the initial concentration influence $\%R_{ap}$. The maximum $\%R_{ap}$ for the experiments grid reached pH 12 in both biomasses. The initial concentrations were 50 and 40 mg/L for NLB and LEB, respectively. Moreover, the maximum $\%R_{ap}$ occurred at a biomass dosage of 60 mg for NLB and 40 mg for LEB.

The linear model fitting results better describe the influence on the **Tc** removal of variables and their interactions (see Table 2). In both cases, NLB and LEB, the models were significant ($p < 1 \times 10^{-4}$) as showed by the ANOVA test. The determination coefficient ($R^2$) was 0.81 and 0.91 for LEB and NLB.

The dependence of **Tc** $\%R_{ap}$ with pH is described as a second-order polynomial. In NLB, the parabola opens upward, and the vertex is at a minimum. There are no interactions with $C_0$ and $m$ (see Table 2). At the $C_0$ and $m$ values, where $\%R_{ap}$ is maximum ($m$ = 60 mg and $C_0$ = 50 mg/L), pH described concave parabolas (see Figure 2a,c). The vertex is close to 4 pH units. This behavior supports the ascending trend observed in Figure 1a.

Conversely, in LEB, the parabola opens downward, and the vertex is a maximum (see Table 2). The interactions with $C_0$ and $m$ revealed antagonist effects, that is, $\%R_{ap}$ increases with the pH, but the increasing $C_0$ and $m$ slow this change rate. At $m$ = 40 mg, pH draws a concave parabola at all studied $C_0$ values with the vertex near 4 pH units (Figure 2b). Although, $\%R_{ap}$ has two opposite behavior depending on pH values. Lower pH favored the ascending trend of $\%R_{ap}$ with the increasing $C_0$. Instead, at higher pH, $\%R_{ap}$ showed an antagonist of $C_0$.

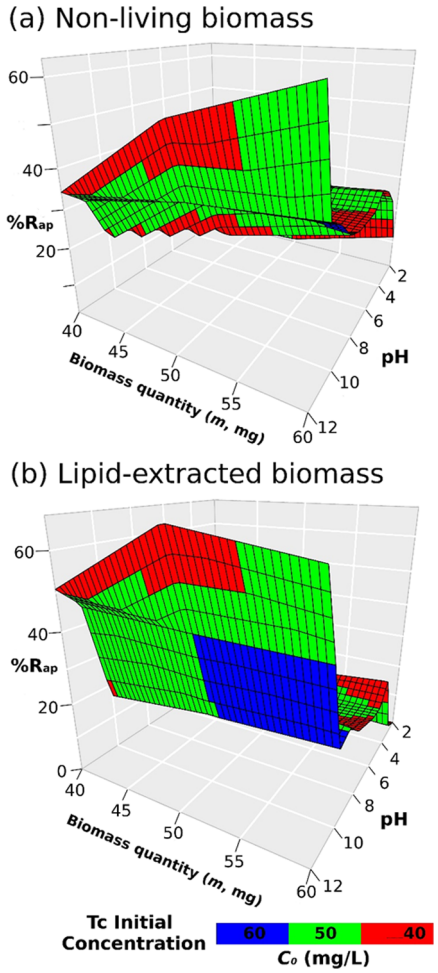


**Figure 1.** Response surface for **Tc** apparent removal ($\%R_{ap}$) with (a) nonliving and (b) lipid-extracted *Chlorella* sp. biomasses.

**Table 2. Linear Regression Models for Response Surface of $\%R_{ap}$ as Function of Initial Concentration ($C_0$), Biosorbent Dosage ($m$), and pH[a]**

| | LEB | | NLB |
|---|---|---|---|
| variable | estimate ± std. error | variable | estimate ± std. error |
| $\%R^0_{ap}$ | 1465 ± 606.5 | $\%R^0_{ap}$ | −11,190 ± 4450 |
| $m$ | 63.02 ± 25.22 | $m$ | 460.9 ± 181.6 |
| $C_0$ | −29.66 ± 11.35 | $C_0$ | 463.7 ± 179.0 |
| pH | 42.81 ± 15.55 | pH | −5.514 ± 2.362 |
| $m^2$ | 0.656 ± 0.254 | $m^2$ | −4.611 ± 1.808 |
| $pH^2$ | −2.481 ± 1.055 | $C_0^2$ | −4.695 ± 1.762 |
| $m \cdot C_0$ | 1.228 ± 0.470 | $pH^2$ | 0.714 ± 0.170 |
| $m \cdot$ pH | −0.884 ± 0.321 | $m \cdot C_0$ | −19.06 ± 7.30 |
| $m^2 \cdot C_0$ | −0.0122 ± 0.0047 | $m^2 \cdot C_0$ | 0.191 ± 0.073 |
| $pH^2 \cdot C_0$ | −0.0111 ± 0.0051 | $m \cdot C_0^2$ | 0.193 ± 0.072 |
| $m \cdot pH^2$ | −0.0673 ± 0.0229 | $m^2 \cdot C_0^2$ | −0.019 ± 0.007 |
| $R^2$ | 0.8123 | $R^2$ | 0.9061 |
| $p$ | $7.53 \times 10^{-5}$ | $p$ | $7.81 \times 10^{-7}$ |

[a]The showed terms have significance lower than 0.05.

Previous studies have shown that pH variations affect the removal of tetracycline depending on the sorbent. Li and Wong found that the adsorption capacity of **Tc** increases with increasing pH by using biomasses of *Pachydictyon coriaceum* and *Sargassum hemiphyllum*.[39] Ding et al. found the maximum



https://doi.org/10.1021/acsomega.2c00696
ACS Omega 2022, 7, 14128−14137

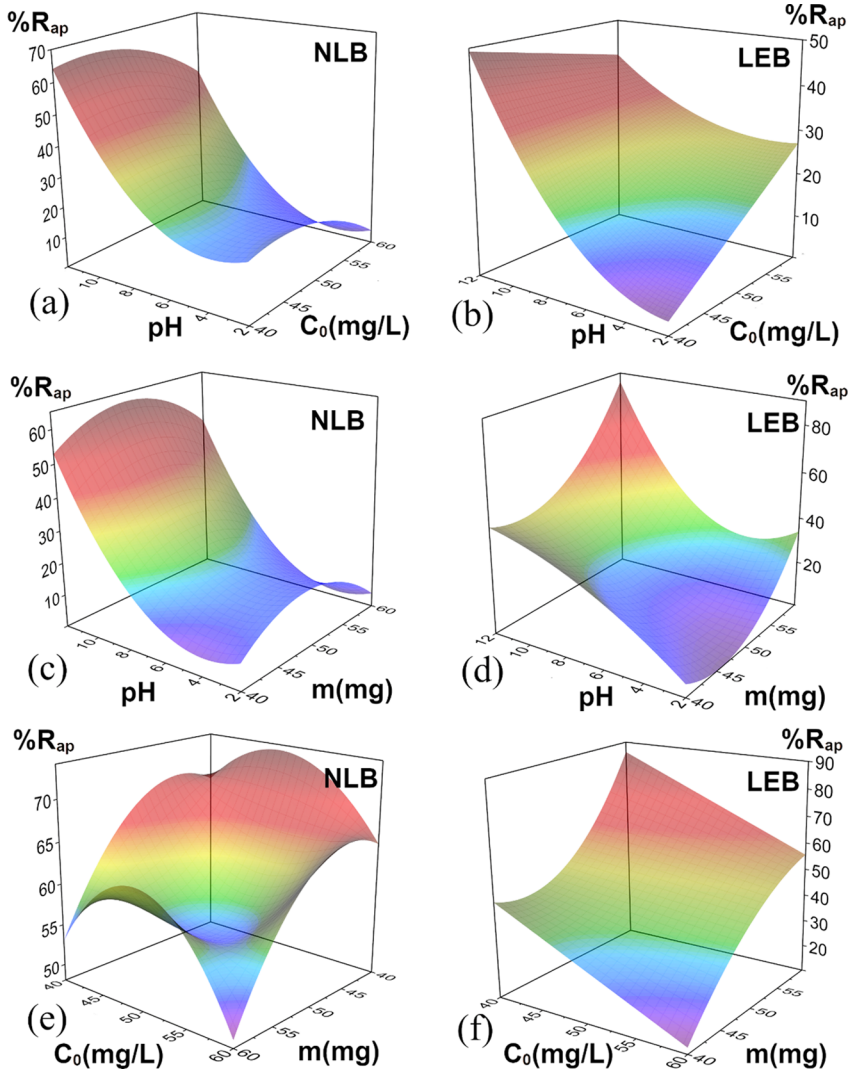


**Figure 2.** Surface response plots of apparent removal of **Tc** with NLB (a, c, e) and NLB (b, d, e). $C_0$ vs pH biplot at $m$ (NLB) = 60 mg (a) and $m$ (LEB) = 40 mg (b). $m$ vs pH biplot at $C_0$ (NLB) = 50 mg/L (c) and $C_0$ (LEB) = 40 mg/L. $m$ vs $C_0$ biplot at pH = 12: (e) NLB and (f) LEB. The $z$-axis is the **Tc** apparent removal.

**Tc** removal at pH between 6 and 8 with dry biomass of acid-treated (and untreated) roots of *Alternanthera philoxeroides*.[40]

On the other hand, Daneshvar et al. reported the maximum **Tc** removal at pH between 8 and 10 with lipid-free *Scenedesmus quadricauda* and *Tetraselmis suecica* biomasses.[27] This behavior evidences the effect of the tetracycline prototropic species—which is in equilibrium at all pH ranges—on adsorbate−adsorbent interaction.[37]

On the other hand, the biomass dosage and the initial concentration had a more complex behavior. In NLB, the linear terms of $C_0$ and $m$ favored the **Tc** $\%R_{ap}$, while the quadratic terms exhibited a reverted role. The negative sign of the interactions between $C_0$ and $m$ suggests an antagonist effect on **Tc** $\%R_{ap}$ with $C_0$ and $m$. Despite the parabolic trend, at pH 12, the removal increases as $C_0$ and $m$ decrease (see Figure 2e). This biomass performed better at lower $C_0$ and $m$. Li and Wong found similar behavior in the efficiency of **Tc** removal using the biomass of *Pachydictyon coriaceum* and *Sargassum hemiphyllum* as biosorbents.[39]

The **Tc** $\%R_{ap}$ in LEB improved with the increasing biomass dosage ($m$), and it is reinforced by the synergy with $C_0$ ($m$, $m^2$, and $m \cdot C_0$ coefficients >0). Conversely, **Tc** $\%R_{ap}$ has an antagonist effect with $C_0$ ($C_0$ coefficient <0) and a complementary effect by the $C_0 \cdot m$ interaction. **Tc** $\%R_{ap}$ increased with the increasing $m$ and the decreasing $C_0$ (see Figure 2e,f). The available adsorption sites grow with the biomass quantity despite the increasing occupation by **Tc**. The defatted biomass of *Scenedesmus quadricauda* and *Tetraselmis suecica* performed similarly to LEB in **Tc** removal below 50 mg/L.[27]

The calibration curve was built with the maximum-removal conditions. The UV−vis spectrum of tetracycline in an aqueous solution at pH 12 revealed two absorption maxima at 269.6 nm ($\lambda_1$) and 379.6 nm ($\lambda_2$) (Figure S1, Supporting Information). According to ANCOVA, there is no significant interaction between the concentration and the treatment ($T$) for both absorption maxima; see Table S1 (Supporting information). The model $A = C \times T$ obtained the significance values of $p$ = 0.731 and 0.660 for 379.6 and 269.6 nm, respectively. Therefore, there are no significant differences in the slopes of the calibration curves between treatments.

The evaluation of models without interaction ($A = C + T$) shows the significance of $T$ in the model ($p < 0.05$), suggesting an effect of $T$ on the intercept of each calibration curve. The



https://doi.org/10.1021/acsomega.2c00696
ACS Omega 2022, 7, 14128−14137

comparison between models with and without interaction revealed a statistically nonsignificant difference between them ($p > 0.05$) at both absorption maxima (see Table S2, Supporting Information). Based on this analysis, it is possible to conclude that there is no matrix effect on the calibration curves. It is noteworthy that the matrix absorption at 379.6 nm is approximately zero, and it was selected as the working wavelength.

**3.2. Removal Efficiency and Adsorption Kinetics.** Table 3 shows the **Tc** removal efficiency for both biomasses.

**Table 3. Time Profile for the Tc Removal Percentage with Nonliving and Lipid-Free *Chlorella sp.* Biomasses**

| $t$ (min) | %$R$ (NLB) | %$R$ (LEB) |
|---|---|---|
| 0 | 0.00 ± 3.3 | 0.00 ± 3.3 |
| 1 | 40.8 ± 2.3 | 34.9 ± 2.4 |
| 15 | 57.7 ± 1.9 | 56.7 ± 1.9 |
| 30 | 60.1 ± 1.8 | 62.5 ± 1.8 |
| 60 | 61.0 ± 1.8 | 66.8 ± 1.7 |
| 120 | 61.0 ± 1.8 | 67.8 ± 1.7 |
| 180 | 67.8 ± 1.7 | 70.4 ± 1.6 |
| 240 | 66.2 ± 1.7 | 69.7 ± 1.6 |
| 300 | 65.8 ± 1.7 | 70.9 ± 1.6 |
| 360 | 68.0 ± 1.7 | 76.9 ± 1.5 |

The concentrations were calculated with the calibration curves and the conditions of maximum removal. In this table, the maximum tetracycline removal for NLB was 68.0%, while LEB removed 76.9%. The absorption capacity is 14.1 (NLB) and 19.2 (LEB) mg/g, confirming the enhanced removal efficiency of the defatted biomass. Also, these results were shown to be superior to those reported by Daneshvar et al. for the lipid-free biomass of *Scenedesmus quadricauda* (62.97% at 80 mg/L) and *Tetraselmis suecica* (55.11% at 80 mg/L).[27] Likewise, our results exceed the removal efficiency of the biosorbents *Sargassum hemiphyllum* (40%) and *Pachydictyon coriaceum* (70%).[39] These results revealed a valorization of the waste from the lipid extraction of the nonliving microalgae biomass, contributing to improving the process's sustainability.

On the other hand, a comparison with activated carbon from macadamia nutshells showed comparable or superior performance of our material (70% at pH = 5 and $C_0$ = 600 mg/L). However, at pH < 5, the removal efficiency was about 80%.[41] Peng et al. reported an enhanced removal efficiency of **Tc** (97.8%) by improving microalgae-based biochar with iron.[42] The advanced adsorption materials as graphene oxide functionalized with magnetic particles[15] and multiwalled carbon nanotubes[16] showed high removal efficiency (86–99.8%), as expected. However, Gao et al. reported 71.4% in **Tc** removal efficiency with graphene oxide showing comparable performance to our inexpensive material.[43]

The fitting of the adsorptive capacity data against time using the different models is shown in Figure 3. The system reached equilibrium after 180 min of contact. A comparison with the literature shows that equilibrium time was 180 and 0 min for lipid-free biomass from *Scenedesmus quadricauda* and *Tetraselmis suecica*, respectively.[27] In other studies with several adsorbates, high variability in equilibrium time was observed. Lin et al. reported 10 min to reach equilibrium in removing **Tc** with graphene oxide functionalized with $Fe_3O_4$ magnetic particles.[15] A Fe activated microalgae-derived biochar reached equilibrium at 60 min.[42] On the other hand, Montmorillonite

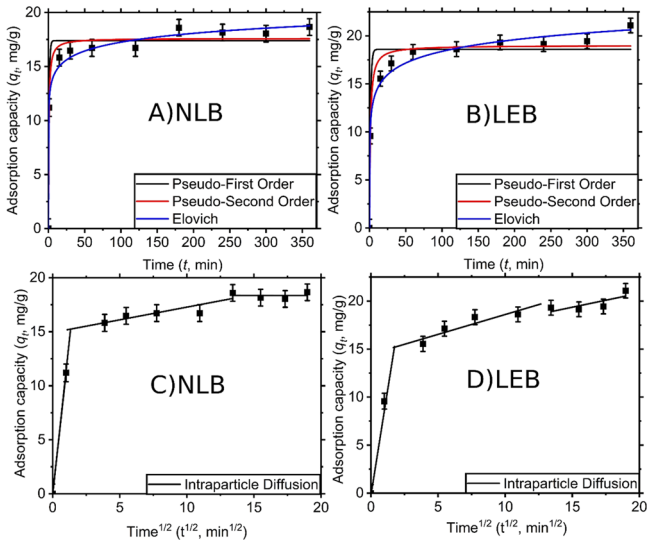


**Figure 3.** Tetracycline adsorption kinetics results using (A, C) nonliving and (B, D) lipid-extracted *Chlorella* sp. biomasses. Pseudo-first-order, pseudo-second-order, and Elovich models are in the upper plots (A and B), and intraparticle diffusion is in the lower plots (C and D). For NLB experiments, **Tc** initial concentration was 50 mg/L and 60 mg of biomass and subsequently, for LEB, **Tc** initial concentration was 40 mg/L and 40 mg of biomass. All experiments were conducted at pH = 12.

with Cu(II) and activated carbon from tomato residues reported high equilibration times, 960 and 2280 min, respectively.[44] Using Illite 2:1 layered clay mineral, Po-Hsiang et al. reported an equilibration time of 8 h.[45]

The goodness-of-fit and regression results are observed in Table 4. According to the determination coefficient, the data fitted to a pseudo-second-order model, $R^2$ = 0.996 (NLB) and $R^2$ = 0.999 (LEB). However, the coefficient of determination showed a good fit for the pseudo-first-order model ($R^2 > 0.9$, see Table 4). The $q_t$ values were also fitted to the Elovich model, $R^2$ = 0.991 (NLB) and $R^2$ = 0.990 (LEB). The pseudo-second-order model could better predict the value of experimental equilibrium adsorption capacity ($q_e$).

These results suggest that adsorption kinetic is mainly controlled by chemisorption. However, the well fitting to pseudo-first-order model allowed us to infer the coexistence of chemical and physical processes.[46] On the other hand, the Elovich model supports the chemisorption mechanism and suggests an interaction between adsorbates.[47]

The intraparticle diffusion model shows that bulk transport occurred up to 5 min of contact (see Figure 3C,D). Furthermore, the film transport has governed the process between 5 and 180 min in NLB, followed by the intraparticle diffusion and adsorption–desorption equilibrium. For LEB, the film transport is observed up to 360 min.

These results agree with SEM morphology and particle and pore size. The small NLB particle is formed by small pores, limiting the film transport and intraparticle diffusion. Consequently, the adsorption equilibrium can reach quickly. Conversely, in LEB, the processes can be slow due to this material's pore size and distribution characteristics.

**3.3. Adsorption Equilibrium.** In Figure 4, the $q_e$ data draw a type III isotherm according to the Brunauer and IUPAC classification. This isotherm describes multilayer



https://doi.org/10.1021/acsomega.2c00696
ACS Omega 2022, 7, 14128–14137

**Table 4. Results for Adsorption Kinetics of Tetracycline in Nonliving *Chlorella* sp.(NLB) and Lipid-Extracted (LEB) Biomasses[a]**

| sorbent | pseudo-first order | | |
|---|---|---|---|
| | $q_e$ (mg·g$^{-1}$) | $k_1$ (min$^{-1}$) | $R^2$ |
| NLB/NLF | 17.4 (4)[b] | 1.03 (18) | 0.970 |
| LEB/NLF | 18.6 (5) | 0.725 (175) | 0.947 |
| | pseudo-second order | | |
| | $q_e$ (mg·g$^{-1}$) | $k_2$ (g·mg$^{-1}$·min$^{-1}$) | $R^2$ |
| NLB/LF | 18.6 (2) | 0.0116 (65) | 0.999 |
| NLB/NLF | 17.6 (3) | 0.0932 (220) | 0.980 |
| LEB/LF | 20.5 (5) | 0.00671 (424) | 0.996 |
| LEB/NLF | 19.0 (5) | 0.0461 (124) | 0.969 |
| | Elovich | | |
| | $\beta$ (mg·g$^{-1}$) | $\alpha$ (mg·g$^{-1}$·min$^{-1}$) | $R^2$ |
| NLB | 0.848 (79) | 2.69 (33.1) × 10$^4$ | 0.991 |
| LEB | 0.572 (45) | 6.42 (81.6) × 10$^2$ | 0.990 |
| | intraparticle diffusion | | |
| | $C$ | $k_p$ (mg·g$^{-1}$·min$^{1/2}$) | $R^2$ |
| NLB(*II*)[c] | 14.5 (1.0) | 0.41 (13) | 0.827 |
| NLB(III) | 15.0 (2.8) | 0.29 (17) | 0.599 |
| LEB(II) | 14.9 (6) | 0.23 (7) | 0.780 |
| LEB(III) | 18.4 (1.5) | −0.0232 | 0.000 |
| | Elovich | | |
| | $\beta$ (mg·g$^{-1}$) | $\alpha$ (mg·g$^{-1}$·min$^{-1}$) | $R^2$ |
| NLB | 0.848 (79) | 2.69 (33.1) × 10$^4$ | 0.991 |
| LEB | 0.572 (45) | 6.42 (81.6) × 10$^2$ | 0.990 |
| | intraparticle diffusion | | |
| | $C$ | $k_p$ (mg·g$^{-1}$·min$^{1/2}$) | $R^2$ |
| NLB(*II*)[c] | 14.5 (1.0) | 0.41 (13) | 0.827 |
| NLB(III) | 15.0 (2.8) | 0.29 (17) | 0.599 |
| LEB(II) | 14.9 (6) | 0.23 (7) | 0.780 |
| LEB(III) | 18.4 (1.5) | −0.0232 | 0.000 |
| | pseudo-second order | | |
| | $q_e$ (mg·g$^{-1}$) | $k_2$ (g·mg$^{-1}$·min$^{-1}$) | $R^2$ |
| NLB/LF | 18.6 (2) | 0.0116 (65) | 0.999 |
| NLB/NLF | 17.6 (3) | 0.0932 (220) | 0.980 |
| LEB/LF | 20.5 (5) | 0.00671 (424) | 0.996 |
| LEB/NLF | 19.0 (5) | 0.0461 (124) | 0.969 |

| | Elovich | | |
|---|---|---|---|
| | $\beta$ (mg·g$^{-1}$) | $\alpha$ (mg·g$^{-1}$·min$^{-1}$) | $R^2$ |
| NLB | 0.848 (79) | 2.69 (33.1) × 10$^4$ | 0.991 |
| LEB | 0.572 (45) | 6.42 (81.6) × 10$^2$ | 0.990 |
| | pseudo-second order | | |
| | $q_e$ (mg·g$^{-1}$) | $k_2$ (g·mg$^{-1}$·min$^{-1}$) | $R^2$ |
| NLB/LF | 18.6 (2) | 0.0116 (65) | 0.999 |
| NLB/NLF | 17.6 (3) | 0.0932 (220) | 0.980 |
| LEB/LF | 20.5 (5) | 0.00671 (424) | 0.996 |
| LEB/NLF | 19.0 (5) | 0.0461 (124) | 0.969 |
| | Elovich | | |
| | $\beta$ (mg·g$^{-1}$) | $\alpha$ (mg·g$^{-1}$·min$^{-1}$) | $R^2$ |
| NLB | 0.848 (79) | 2.69 (33.1) × 10$^4$ | 0.991 |
| LEB | 0.572 (45) | 6.42 (81.6) × 10$^2$ | 0.990 |
| | intraparticle diffusion | | |
| | $C$ | $k_p$ (mg·g$^{-1}$·min$^{1/2}$) | $R^2$ |
| NLB(*II*)[c] | 14.5 (1.0) | 0.41 (13) | 0.827 |
| NLB(III) | 15.0 (2.8) | 0.29 (17) | 0.599 |
| LEB(II) | 14.9 (6) | 0.23 (7) | 0.780 |
| LEB(III) | 18.4 (1.5) | −0.0232 | 0.000 |
| | Elovich | | |
| | $\beta$ (mg·g$^{-1}$) | $\alpha$ (mg·g$^{-1}$·min$^{-1}$) | $R^2$ |
| NLB | 0.848 (79) | 2.69 (33.1) × 10$^4$ | 0.991 |
| LEB | 0.572 (45) | 6.42 (81.6) × 10$^2$ | 0.990 |
| | intraparticle diffusion | | |
| | $C$ | $k_p$ (mg·g$^{-1}$·min$^{1/2}$) | $R^2$ |
| NLB(*II*)[c] | 14.5 (1.0) | 0.41 (13) | 0.827 |
| NLB(III) | 15.0 (2.8) | 0.29 (17) | 0.599 |
| LEB(II) | 14.9 (6) | 0.23 (7) | 0.780 |
| LEB(III) | 18.4 (1.5) | −0.0232 | 0.000 |

[a]LF, linear fit; NLF, nonlinear fit; ID, intraparticle diffusion. [b]This notation is the compact uncertainty notation, that is, X.XX(Y) signifies X.XX ± 0.0Y. [c]Intraparticle diffusion stages: Zone I from $t$ = 0 to 5 min, Zone II from $t$ = 5 to 180 min, and Zone III after 180 min.

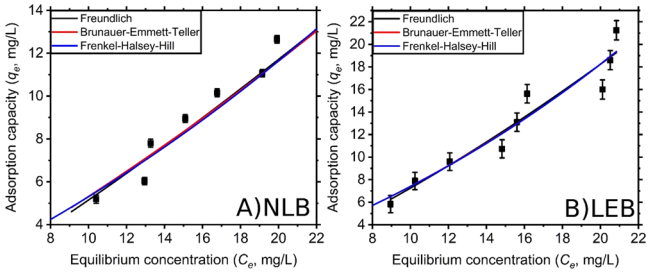


**Figure 4.** Tetracycline adsorption isotherms for (A) nonliving and (B) lipid-extracted *Chlorella* sp. biomasses. NLB experiments were conducted with 60 mg of biomass, while LEB experiments were conducted with 40 mg of biomass. All experiments were conducted at initial pH 12.

adsorption by weak interactions with low energy on a macroporous surface.

The parameters obtained by fitting the data to the isotherm models of Freundlich, Frenkel−Halsey−Hill and BET are shown in Table 5, and the fitted curves are shown in Figure 4. The type III isotherms should not fit the Langmuir isotherm (type II). The three equations can explain the result, suggesting adsorption on a heterogeneous surface. The values of the Freundlich constant ($K_F$) revealed unfavorable adsorption ($K_F$ < 1). NLB (0.339 mg/g) has a similar behavior to LEB (0.336 mg/g. Also, the $1/n$ values mean lower adsorbate−adsorbent affinity in NLB than LEB.

Although **Tc** removal studies in the literature reported Langmuir and Freundlich isotherms, we have taken the Freundlich isotherm results. Comparing algae-based materials shows unfavorable adsorption and low affinity concerning reported values (see Table 5). Similar behavior was observed compared with the biomass of alligator weed roots.[40] As expected, more advanced materials, for example, biochar,[48] activated carbons,[41,49] and graphene oxide,[15,43] had better affinities.

The FHH model represents multilayer adsorption on the surface, assuming a variation of the adsorption potential with distance from the surface.[50] The values of $A_{fhh}$ revealed similar



https://doi.org/10.1021/acsomega.2c00696
ACS Omega 2022, 7, 14128−14137

**Table 5. Results of Adsorption Isotherms of Tetracycline with Nonliving and Defatted *Chlorella* Sp. Biomasses[ab]**

| sorbent/fit method | Freundlich isotherm | | |
|---|---|---|---|
| | $K_F$ (mg·g$^{-1}$) | $1/n$ | $R^2$ |
| NLB | 0.339(166) | 1.33(13) | 0.924 |
| LEB | 0.336(117) | 1.19(10) | 0.945 |
| *Sargassum hemiphyllum*[39] | 0.73 | 0.515 | 0.982 |
| *Pachydictyon coriaceum*[39] | 2.40 | 0.476 | 0.991 |
| *Scenedesmus quadricauda*[27] | 1.97 | 0.779 | 0.987 |
| *Tetraselmis suecica*[27] | 1.51 | 0.749 | 0.993 |
| alligator weed root[40] | 0.94 | 0.52 | 0.995 |
| acid-treated alligator weed root[40] | 0.00137 | 0.73 | 0.967 |
| | Frenkel–Halsey–Hill isotherm | | |
| | $A_{fhh}$ | $B_{fhh}$ | $C_s$ (mg·L$^{-1}$) | $R^2$ |
| NLB/GA + BFGS[c] | 6.026 | 0.2159 | 500 | 0.921 |
| LEB/GA + BFGS[c] | 5.918 | 0.2481 | 500 | 0.962 |
| | BET isotherm | | | |
| | $q_{max}$ (mg·g$^{-1}$) | $C_{BET}$ (L·mg$^{-1}$) | $C_s$ (mg·L$^{-1}$) | $R^2$ |
| NLB/GA + BFGS | 439.1 | 0.144 | 103.6 | 0.923 |
| LEB/GA + BFGS | 1151 | 0.096 | 226.8 | 0.939 |
| | Frenkel–Halsey–Hill isotherm | | | |
| | $A_{fhh}$ | $B_{fhh}$ | $C_s$ (mg·L$^{-1}$) | $R^2$ |
| NLB/GA + BFGS[c] | 6.026 | 0.2159 | 500 | 0.921 |
| LEB/GA + BFGS[c] | 5.918 | 0.2481 | 500 | 0.962 |
| | BET isotherm | | | |
| | $q_{max}$ (mg·g$^{-1}$) | $C_{BET}$ (L·mg$^{-1}$) | $C_s$ (mg·L$^{-1}$) | $R^2$ |
| NLB/GA + BFGS | 439.1 | 0.144 | 103.6 | 0.923 |
| LEB/GA + BFGS | 1151 | 0.096 | 226.8 | 0.939 |

[a]NLB, nonliving biomass. [b]LEB, lipid-extracted biomass. [c]Data fitted with genetic algorithms followed by optimization with Broyden–Fletcher–Goldfarb–Shanno algorithm.

surface adsorption capacity of LEB and NLB. It is associated with long-range interactions between the surface and the first layer and the interaction between adsorbates (as also suggested by the Elovich kinetics). According to these results, in Table 5, the interactions between tetracycline and LEB surface are slightly weaker than NLB. The $B_{fhh}$ values give the interaction between the first layer with the subsequent layers. In our work, these values showed that the tetracycline multilayer is thinner in NLB than the multilayer in LEB, supporting the observed greater removal capacity of the latter (see Table 5).

The BET isotherm reinforced the behavior related to the adsorptive capacity of tetracycline on NLB and LEB—the $q_{max}$ and $C_s$ values are greater in the latter. However, the $C_{BET}$ value suggested that multilayer formation is more favored in LEB (see Table 5). $C_{BET}$ parameter is the relationship between the equilibrium constants of the first layer and subsequent layer formation.[51]

**3.4. Adsorption Mechanism.** According to Figure 2, the **Tc** removal capacity increases with the increasing pH. The biomass compositions are proteins, saccharides, and lipids. The functional groups contained in the surface and interstices are capable of exchanging ions with the media. Then, the surface charge changes depending on these functional groups. The surface acts as a buffer stabilizing the media pH. Daneshvar et al. found the pH ranged between 6.86 and 7.75 after the contact of the biomass with **Tc** solutions at initial pH of 4–10.[27]

On the other hand, **Tc** modifies its electrostatic potential due to the prototopic species governing at a given pH. Figure 5

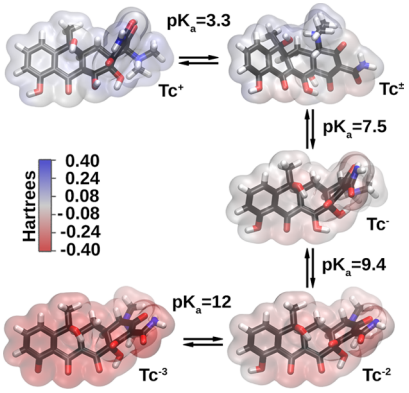


**Figure 5.** Molecular electrostatic potential of tetracycline at different pHs.

shows the electrostatic potential surface of the **Tc** prototopic species. At low pH, the positively charged specie is the more abundant in the media. The positive charge is located at the ammonium and amine groups (~0.172 Hartrees, see Figure 5). The zwitterion species dominate under 7.5 pH units, and the electrostatic potential increased in negative sites and decreased in positive regions (~0.112 Hartrees). As the pH increases (>7.5), the negative electrostatic potential grows around the oxygens forming a keto-enol system.

The high electrostatic potential values promote the electrostatic interactions and the ionic exchange (induced by the aqueous media). The former suggests physisorption, while the second suggests chemisorption. The Elovich model fitting supports the presence of the chemisorption mechanism and, additionally, indicates interactions between adsorbates. The tetracycline self-association inside proteins has been observed.[52] These facts support the observed in the isotherm and kinetic models, justifying the multilayer formation.

At pH around 7, the zwitterion species can interact with positive and negative sites on the surface. The lipid extraction procedure probably decreased the number of negative sites and, consequently, increased the proportion of positive sites. These conditions favored the Tc interaction based on the molecule's rich negative electrostatic potential regions.

The dependence of the adsorption process on pH could provide insights into the desorption mechanism. Figure 3 revealed that desorption starts from 300 min. The charge compensation in the multilayer probably reduces the active sites and modifies the bulk pH. In Figure 2, low pH decreased the removal efficiency.

## 4. CONCLUSIONS

In this work, we have explored the adsorptive capacity of nonliving *Chlorella* sp. biomass before (NLB) and after (LEB) a lipid extraction procedure. In this case, tetracycline from highly concentrated aqueous media was removed. LEB removed 76.9% ($q$ = 19.2 mg/g) of tetracycline at 40 mg/L initial concentration, while NLB removed 68.0% ($q$ = 14.2 mg/g) at 60 mg/L of tetracycline. These results revealed an enhanced removal capacity by LEB compared with NLB and other microalgae-based materials. On the other hand, the adsorption kinetics followed the pseudo-second-order and Elovich models suggesting chemisorption with interactions


https://doi.org/10.1021/acsomega.2c00696
ACS Omega 2022, 7, 14128–14137

between adsorbates. The adsorption isotherms indicate a multilayer mechanism on a heterogeneous surface. Additionally, the interactions between the surface and the first layer of tetracycline are weak, and the formation of the subsequent layers is favored. Microalgae are recognized as a lipid source for food, cosmetics, and biofuel. The byproduct from the lipid extraction procedure removed better tetracycline than the nonprocessed biomass. The *Chlorella* sp. biomass after the lipid extraction process is a promising material for removing tetracycline. Moreover, the use of this residual biomass contributes to the zero-waste strategy.

## ■ ASSOCIATED CONTENT

### Supporting Information

The Supporting Information is available free of charge at https://pubs.acs.org/doi/10.1021/acsomega.2c00696.

UV−vis spectral data of calibration curve (Figure S1) and analysis of covariance comparing the treatment effect on calibration curves (Tables S1 and S2) (PDF)

## ■ AUTHOR INFORMATION


### Corresponding Author

**Néstor Cubillán** − *Grupo de Investigación de Biotecnología de Microalgas, Fisicoquímica Aplicada y Estudios Ambientales, Facultad de Ciencias Básicas, Universidad del Atlántico, Barranquilla 1890, Colombia;* orcid.org/0000-0001-8802-280X; Email: nestorcubillan@mail.uniatlantico.edu.co

### Authors

**Dayra Suárez-Martínez** − *Grupo de Investigación de Biotecnología de Microalgas, Fisicoquímica Aplicada y Estudios Ambientales, Facultad de Ciencias Básicas, Universidad del Atlántico, Barranquilla 1890, Colombia*

**Edgardo Angulo-Mercado** − *Grupo de investigación Bioprocesos, Facultad de Ingeniería, Universidad del Atlántico, Barranquilla 1890, Colombia*

**Ivan Mercado-Martínez** − *Programa de Ingeniería Agroindustrial, Facultad de Ingeniería, Universidad del Atlántico, Barranquilla 1890, Colombia*

**Victor Vacca-Jimeno** − *Grupo de Investigación de Biotecnología de Microalgas, Fisicoquímica Aplicada y Estudios Ambientales, Facultad de Ciencias Básicas, Universidad del Atlántico, Barranquilla 1890, Colombia*

**Claudia Tapia-Larios** − *Grupo de Investigación en Gestión Ecológica y Ambiental, Programa de Microbiología, Facultad de Ciencias Exactas y Naturales, Universidad Libre, Barranquilla 1890, Colombia;* orcid.org/0000-0001-6522-3799

Complete contact information is available at: https://pubs.acs.org/10.1021/acsomega.2c00696


### Notes

The authors declare no competing financial interest.

## ■ ACKNOWLEDGMENTS

The authors thank Ministerio de Ciencias, Tecnología e Innovación (Colombia) by financial support through the Project "Remoción de antibióticos mediante la biomasa residual de microalgas después de extracción de lípidos" (grant number: 64514).

## ■ REFERENCES


(1) Grossman, T. H. Tetracycline Antibiotics and Resistance. *Cold Spring Harb. Perspect. Med.* **2016**, *6*, No. a025387.

(2) Carvalho, I. T.; Santos, L. Antibiotics in the Aquatic Environments: A Review of the European Scenario. *Environ. Int.* **2016**, *94*, 736−757.

(3) Granados-Chinchilla, F.; Rodríguez, C. Tetracyclines in Food and Feedingstuffs: From Regulation to Analytical Methods, Bacterial Resistance, and Environmental and Health Implications. *J. Anal. Methods Chem.* **2017**, *2017*, No. 1315497.

(4) Ziółkowski, H.; Jasiecka-Mikołajczyk, A.; Madej-Śmiechowska, H.; Janiuk, J.; Zygmuntowicz, A.; Dąbrowski, M. Comparative Pharmacokinetics of Chlortetracycline, Tetracycline, Minocycline and Tigecycline in Broiler Chickens. *Poult. Sci.* **2020**, *99*, 4750−4757.

(5) Michael, C. A.; Dominey-Howes, D.; Labbate, M. The Antimicrobial Resistance Crisis: Causes, Consequences, and Management. *Front. Public Health* **2014**, *2*, 145.

(6) Javid, A.; Mesdaghinia, A.; Nasseri, S.; Mahvi, A. H.; Alimohammadi, M.; Gharibi, H. Assessment of Tetracycline Contamination in Surface and Groundwater Resources Proximal to Animal Farming Houses in Tehran, Iran. *J. Environ. Health Sci. Eng.* **2016**, *14*, 4.

(7) Wang, Z.; Chen, Q.; Zhang, J.; Dong, J.; Yan, H.; Chen, C.; Feng, R. Characterization and Source Identification of Tetracycline Antibiotics in the Drinking Water Sources of the Lower Yangtze River. *J. Environ. Manage.* **2019**, *244*, 13−22.

(8) Kim, Y. B.; Seo, K. W.; Jeon, H. Y.; Lim, S. K.; Sung, H. W.; Lee, Y. J. Molecular Characterization of Erythromycin and Tetracycline-Resistant Enterococcus Faecalis Isolated from Retail Chicken Meats. *Poult. Sci.* **2019**, *98*, 977−983.

(9) Pena, A.; Paulo, M.; Silva, L. J. G.; Seifrtová, M.; Lino, C. M.; Solich, P. Tetracycline Antibiotics in Hospital and Municipal Wastewaters: A Pilot Study in Portugal. *Anal. Bioanal. Chem.* **2010**, *396*, 2929−2936.

(10) Yi, Q.; Gao, Y.; Zhang, H.; Zhang, H.; Zhang, Y.; Yang, M. Establishment of a Pretreatment Method for Tetracycline Production Wastewater Using Enhanced Hydrolysis. *Chem. Eng. J.* **2016**, *300*, 139−145.

(11) Liu, H.; Xu, G.; Li, G. Preparation of Porous Biochar Based on Pharmaceutical Sludge Activated by NaOH and Its Application in the Adsorption of Tetracycline. *J. Colloid Interface Sci.* **2021**, *587*, 271−278.

(12) Daghrir, R.; Drogui, P. Tetracycline Antibiotics in the Environment: A Review. *Environ. Chem. Lett.* **2013**, *11*, 209−227.

(13) Zhang, N.; Chen, J.; Fang, Z.; Tsang, E. P. Ceria Accelerated Nanoscale Zerovalent Iron Assisted Heterogenous Fenton Oxidation of Tetracycline. *Chem. Eng. J.* **2019**, *369*, 588−599.

(14) Zhang, S.; Song, H.; Yang, X.; Yang, K.; Wang, X. Effect of Electrical Stimulation on the Fate of Sulfamethoxazole and Tetracycline with Their Corresponding Resistance Genes in Three-Dimensional Biofilm-Electrode Reactors. *Chemosphere* **2016**, *164*, 113−119.

(15) Lin, Y.; Xu, S.; Li, J. Fast and Highly Efficient Tetracyclines Removal from Environmental Waters by Graphene Oxide Functionalized Magnetic Particles. *Chem. Eng. J.* **2013**, *225*, 679−685.

(16) Zhang, L.; Song, X.; Liu, X.; Yang, L.; Pan, F.; Lv, J. Studies on the Removal of Tetracycline by Multi-Walled Carbon Nanotubes. *Chem. Eng. J.* **2011**, *178*, 26−33.

(17) Bernaerts, T. M. M.; Gheysen, L.; Kyomugasho, C.; Jamsazzadeh Kermani, Z.; Vandionant, S.; Foubert, I.; Hendrickx, M. E.; Van Loey, A. M. Comparison of Microalgal Biomasses as Functional Food Ingredients: Focus on the Composition of Cell Wall Related Polysaccharides. *Algal Res.* **2018**, *32*, 150−161.

(18) Menegazzo, M. L.; Fonseca, G. G. Biomass Recovery and Lipid Extraction Processes for Microalgae Biofuels Production: A Review. *Renew. Sustain. Energy Rev.* **2019**, *107*, 87−107.

(19) De Luca, M.; Pappalardo, I.; Limongi, A. R.; Viviano, E.; Radice, R. P.; Todisco, S.; Martelli, G.; Infantino, V.; Vassallo, A.

Lipids from Microalgae for Cosmetic Applications. *Cosmetics* **2021**, *8*, 52.
(20) Costa, J. A. V.; Freitas, B. C. B.; Moraes, L.; Zaparoli, M.; Morais, M. G. Progress in the Physicochemical Treatment of Microalgae Biomass for Value-Added Product Recovery. *Bioresour. Technol.* **2020**, *301*, No. 122727.
(21) Ye, C.; Mu, D.; Horowitz, N.; Xue, Z.; Chen, J.; Xue, M.; Zhou, Y.; Klutts, M.; Zhou, W. Life Cycle Assessment of Industrial Scale Production of Spirulina Tablets. *Algal Res.* **2018**, *34*, 154−163.
(22) Hanifzadeh, M.; Sarrafzadeh, M.-H.; Nabati, Z.; Tavakoli, O.; Feyzizarnagh, H. Technical, Economic and Energy Assessment of an Alternative Strategy for Mass Production of Biomass and Lipid from Microalgae. *J. Environ. Chem. Eng.* **2018**, *6*, 866−873.
(23) Nautiyal, P.; Subramanian, K. A.; Dastidar, M. G. Experimental Investigation on Adsorption Properties of Biochar Derived from Algae Biomass Residue of Biodiesel Production. *Environ. Process.* **2017**, *4*, 179−193.
(24) Sutherland, D. L.; Ralph, P. J. Microalgal Bioremediation of Emerging Contaminants - Opportunities and Challenges. *Water Res.* **2019**, *164*, No. 114921.
(25) Hena, S.; Gutierrez, L.; Croué, J. P. Removal of Pharmaceutical and Personal Care Products (PPCPs) from Wastewater Using Microalgae: A Review. *J. Hazard. Mater.* **2021**, *403*, No. 124041.
(26) Angulo, E.; Bula, L.; Mercado, I.; Montaño, A.; Cubillán, N. Bioremediation of Cephalexin with Non-Living Chlorella Sp., Biomass after Lipid Extraction. *Bioresour. Technol.* **2018**, *257*, 17−22.
(27) Daneshvar, E.; Zarrinmehr, M. J.; Hashtjin, A. M.; Farhadian, O.; Bhatnagar, A. Versatile Applications of Freshwater and Marine Water Microalgae in Dairy Wastewater Treatment, Lipid Extraction and Tetracycline Biosorption. *Bioresour. Technol.* **2018**, *268*, 523−530.
(28) Saldaña, K.; Angulo, E.; Mercado, I.; Castellar, G.; Cubillán, N. Removal of Minocycline from High Concentrated Aqueous Medium by Nonliving and Lipid-Free Chlorella Sp. Biomass. *Bioresour. Technol. Rep.* **2022**, *17*, No. 100921.
(29) Hosseinizand, H.; Sokhansanj, S.; Lim, C. J. Studying the Drying Mechanism of Microalgae Chlorella Vulgaris and the Optimum Drying Temperature to Preserve Quality Characteristics. *Dry. Technol.* **2018**, *36*, 1049−1060.
(30) Bligh, E. G.; Dyer, W. J. A Rapid Method Of Total Lipid Extraction And Purification. *Can. J. Biochem. Physiol.* **1959**, *37*, 911−917.
(31) Guo, X.; Su, G.; Li, Z.; Chang, J.; Zeng, X.; Sun, Y.; Lu, Y.; Lin, L. Light Intensity and N/P Nutrient Affect the Accumulation of Lipid and Unsaturated Fatty Acids by Chlorella Sp. *Bioresour. Technol.* **2015**, *191*, 385−390.
(32) D'Oca, M. G. M.; Viêgas, C.; Lemões, J.; Miyasaki, E.; Morón-Villarreyes, J.; Primel, E.; Abreu, P. Production of FAMEs from Several Microalgal Lipidic Extracts and Direct Transesterification of the Chlorella Pyrenoidosa. *Biomass Bioenergy* **2011**, *35*, 1533−1538.
(33) Wheeler, R. AlgDesign. *The R Foundation for statistical computing* 2004.
(34) R Core Team. *R: A Language and Environment for Statistical Computing*; R Foundation for Statistical Computing: Vienna, Austria, 2018.
(35) McKay, G.; Otterburn, M. S.; Sweeney, A. G. The Removal of Colour from Effluent Using Various Adsorbents-III. Silica: Rate Processes. *Water Res.* **1980**, *14*, 15−20.
(36) Scrucca, L. On Some Extensions to GA Package: Hybrid Optimisation, Parallelisation and Islands Evolution. *R J.* **2017**, *9*, 187.
(37) Jin, L.; Amaya-Mazo, X.; Apel, M. E.; Sankisa, S. S.; Johnson, E.; Zbyszynska, M. A.; Han, A. Ca2+ and Mg2+ Bind Tetracycline with Distinct Stoichiometries and Linked Deprotonation. *Biophys. Chem.* **2007**, *128*, 185−196.
(38) Frisch, M. J.; Trucks, G. W.; Schlegel, H. B.; Scuseria, G. E.; Robb, M. A.; Cheeseman, J. R.; Scalmani, G.; Barone, V.; Mennucci, B.; Petersson, G. A.; Nakatsuji, H.; Li, X.; Caricato, M.; Marenich, A. V.; Bloino, J.; Janesko, B. G.; Gomperts, R.; Hratchian, H. P.; Ortiz, J. V.; Izmaylov, A. F.; Sonnenberg, J. L.; Williams-Young, D.; Ding, F.; Lipparini, F.; Egidi, F.; Goings, J.; Peng, B.; Petrone, A.; Henderson, T.; Ranasinghe, D.; Zakrzewski, V. G.; Gao, J.; Rega, N.; Zheng, G.; Liang, W.; Hada, M.; Ehara, M.; Toyota, K.; Fukuda, R.; Hasegawa, J.; Ishida, M.; Nakajima, T.; Honda, Y.; Kitao, O.; Nakai, H.; Vreven, T.; Throssell, K.; Montgomery, J. A., Jr.; Peralta, J. E.; Ogliaro, F.; Bearpark, M. J.; Heyd, J. J.; Brothers, E. N.; Kudin, K. N.; Staroverov, V. N.; Keith, T. A.; Kobayashi, R.; Normand, J.; Raghavachari, K.; Rendell, A. P.; Burant, J. C.; Iyengar, S. S.; Tomasi, J.; Cossi, M.; Millam, J. M.; Klene, M.; Adamo, C.; Cammi, R.; Ochterski, J. W.; Martin, R. L.; Morokuma, K.; Farkas, O.; Foresman, J. B.; Fox, D. J. *Gaussian 09 Revision A.2*; Wallingford, 2009.
(39) Li, W. C.; Wong, M. H. A Comparative Study on Tetracycline Sorption by Pachydictyon Coriaceum and Sargassum Hemiphyllum. *Int. J. Environ. Sci. Technol.* **2015**, *12*, 2731−2740.
(40) Ding, Y. Y.; Cui, H.; Chen, J. Biosorption of Tetracycline onto Dried Alligator Weed Root: Effect of Solution Chemistry and Role of Metal (Hydr)Oxides. *Res. Chem. Intermed.* **2017**, *43*, 1121−1138.
(41) Martins, A. C.; Pezoti, O.; Cazetta, A. L.; Bedin, K. C.; Yamazaki, D. A. S. S.; Bandoch, G. F. G. G.; Asefa, T.; Visentainer, J. V.; Almeida, V. C. Removal of Tetracycline by NaOH-Activated Carbon Produced from Macadamia Nut Shells: Kinetic and Equilibrium Studies. *Chem. Eng. J.* **2015**, *260*, 291−299.
(42) Peng, L.; Ren, Y.; Gu, J.; Qin, P.; Zeng, Q.; Shao, J.; Lei, M.; Chai, L. Iron Improving Bio-Char Derived from Microalgae on Removal of Tetracycline from Aqueous System. *Environ. Sci. Pollut. Res.* **2014**, *21*, 7631−7640.
(43) Gao, Y.; Li, Y.; Zhang, L.; Huang, H.; Hu, J.; Shah, S.; Su, X. Adsorption and Removal of Tetracycline Antibiotics from Aqueous Solution by Graphene Oxide. *J. Colloid Interface Sci.* **2012**, *368*, 540−546.
(44) Wang, Y. U. J.; Jia, D. E. A. N.; Sun, R. J.; Zhu, H. W.; Zhou, D. M. Adsorption and Cosorption of Tetracycline and Copper (Ll) on Montmorillonite as Affected by Solution PH. *Environ. Sci. Technol.* **2008**, *42*, 3254−3259.
(45) Chang, P. H.; Li, Z.; Jean, J. S.; Jiang, W. T.; Wang, C. J.; Lin, K. H. Adsorption of Tetracycline on 2:1 Layered Non-Swelling Clay Mineral Illite. *Appl. Clay Sci.* **2012**, *67-68*, 158−163.
(46) Yang, X.; Xu, G.; Yu, H.; Zhang, Z. Preparation of Ferric-Activated Sludge-Based Adsorbent from Biological Sludge for Tetracycline Removal. *Bioresour. Technol.* **2016**, *211*, 566−573.
(47) Largitte, L.; Pasquier, R. A Review of the Kinetics Adsorption Models and Their Application to the Adsorption of Lead by an Activated Carbon. *Chem. Eng. Res. Des.* **2016**, *109*, 495−504.
(48) Jang, H. M.; Yoo, S.; Choi, Y.-K.; Park, S.; Kan, E. Adsorption Isotherm, Kinetic Modeling and Mechanism of Tetracycline on Pinus Taeda-Derived Activated Biochar. *Bioresour. Technol.* **2018**, *259*, 24−31.
(49) Pan, L.; Cao, Y.; Zang, J.; Huang, Q.; Wang, L.; Zhang, Y.; Fan, S.; Tang, J.; Xie, Z. Preparation of Iron-Loaded Granular Activated Carbon Catalyst and Its Application in Tetracycline Antibiotic Removal from Aqueous Solution. *Int. J. Environ. Res. Public Health* **2019**, *16*, 2270.
(50) Saadi, R.; Saadi, Z.; Fazaeli, R.; Fard, N. E. Monolayer and Multilayer Adsorption Isotherm Models for Sorption from Aqueous Media. *Korean J. Chem. Eng.* **2015**, *32*, 787−799.
(51) Ebadi, A.; Soltan Mohammadzadeh, J. S.; Khudiev, A. What Is the Correct Form of BET Isotherm for Modeling Liquid Phase Adsorption? *Adsorption* **2009**, *15*, 65−73.
(52) Dalm, D.; Palm, G. J.; Aleksandrov, A.; Simonson, T.; Hinrichs, W. Nonantibiotic Properties of Tetracyclines: Structural Basis for Inhibition of Secretory Phospholipase A2. *J. Mol. Biol.* **2010**, *398*, 83−96.


https://doi.org/10.1021/acsomega.2c00696
*ACS Omega* 2022, 7, 14128−14137